Biomaterials Science

PAPER

View Article Online
View Journal | View Issue



Cite this: *Biomater. Sci.*, 2017, **5**, 1558

# Phosphatase-triggered cell-selective release of a Pt(IV)-backboned prodrug-like polymer for an improved therapeutic index†

Shao-Lu Li,‡[a] Yingqin Hou,‡[a] Yali Hu,[a] Jin Yu,[a] Wei Wei*[b] and Hua Lu*[a]

Received 22nd December 2016,
Accepted 2nd February 2017

DOI: 10.1039/c6bm00935b

rsc.li/biomaterials-science

We describe here the synthesis and cell-selective delivery of a cationic Pt(IV)-backboned prodrug-like polymer P(DSP-DAEP). P(DSP-DAEP) features excellent aqueous solubility, unusually high (44.5%) drug loading, can be rapidly reduced to release the active cisplatin, and is more potent than its small molecular Pt(IV) precursor DSP. P(DSP-DAEP) can be formulated with an oppositely charged methoxyl poly(ethylene glycol)-*block*-poly(L-phosphotyrosine) (mPEG-*b*-PpY) to afford a polyion micelle (Pt-PIC) by taking advantage of polyelectrolyte coacervation. Preliminary *in vitro* cellular uptake and cytotoxicity assays indicate that Pt-PIC exhibits receptor (surface alkaline phosphatase)-dependent uptake and cytotoxicity. Overall, our results suggest a new approach to the improved therapeutic index of platinum-based anticancer drugs *via* cell-selective delivery.



## Introduction

Cisplatin, or *cis*-diamminedichloridoplatinum(II) (CDDP), is a more-than-forty-years-old chemotherapy drug for lung, gastrointestinal and genitourinary cancers.[1] Despite its broad clinical application, CDDP often leads to severe side-effects such as nephrotoxicity and neurotoxicity, which necessitates drug delivery systems for an improved therapeutic index.[2–11] Moreover, because of the intrinsically labile square-planar structure of Pt(II), CDDP can undergo rapid ligand exchange with water and sulfur-containing small molecular ligands (*e.g.* GSH) before it takes effect. To improve the therapeutic window of CDDP, the six-coordinated Pt(IV) compounds have emerged as promising prodrugs because they are less toxic and more inert in a biological environment than Pt(II) species. In the intracellular reductive environment, these Pt(IV) compounds can be activated by regenerating the anticancer Pt(II) species.[12–23] Importantly, the octahedral Pt(IV) prodrugs have two additional "axial" ligand sites compared to Pt(II) drugs, which offer convenient chemical handles for further functionalization.[24,25] In the past decade, many Pt(IV) prodrugs[19,23,26,27] and delivery systems have been developed including single walled carbon nanotubes,[12] gold nanoparticles,[14] polymeric nanoparticles,[18,28] and Pt(IV) nanoscale coordination polymers (NCPs) coated with a silica or liposome surface.[13,29–31] For polymeric delivery systems, the Pt(IV) moieties are typically attached at their chain ends or pendant side chains.[32,33] This strategy, however, usually gives inconsistent and varied drug loading as low as 1 wt%.[28] Considering the utmost importance of a high drug loading to the success of a delivery system,[34,35] we reason that drug-backboned polymers, which can afford predictable and reproducibly high drug loading, may be superior to the aforementioned conventional ones bearing Pt(IV) on the side chains.[36–38] Indeed, Shen and coworkers reported for the first time a series of Pt(IV)-backboned polymers, which showed high Pt loading ranging from 10 to 29%.[39] However, a further increase of drug loading may lead to hampered solubility and aggregation of these drug-backboned polymers.

To further expand the therapeutic window of CDDP, targeted delivery has been a longstanding strategy. For this, two approaches are frequently adapted namely the passive targeting that harnesses the so called enhanced permeation and retention (EPR) effect, and the active targeting by using ligands that recognize tumor specific/associated receptors.[18] For example, ligands such as aptamers,[40,41] RGD/iRGD peptides,[42–44] folate,[37] anisamide,[45] and glucose[46] have been extensively exploited for cell-selective platinum delivery. More recently, delivery vehicles have been engineered to accumulate and release drugs in response to pathological biomolecules

[a]*Beijing National Laboratory for Molecular Sciences, Center for Soft Matter Science and Engineering, Key Laboratory of Polymer Chemistry and Physics of Ministry of Education, College of Chemistry and Molecular Engineering, Peking University, Beijing 100871, People's Republic of China. E-mail: chemhualu@pku.edu.cn*
[b]*State Key Laboratory of Biochemical Engineering, Institute of Process Engineering, Chinese Academy of Sciences, Beijing, 10090, People's Republic of China. E-mail: weiwei@ipe.ac.cn*

†Electronic supplementary information (ESI) available. See DOI: 10.1039/c6bm00935b

‡These authors contributed equally.

presented in the tumor microenvironment such as matrix metalloproteinase (MMP), hyaluronidase or low pH.[47–52] In this regard, protein tyrosine phosphatase (PTP), whose overexpression and aberrant phosphate-cleavage activity have been correlated with the malignancy of many diseases including cancers,[53,54] has emerged as a potential extracellular cue for tumor microenvironment delivery. However, it is only recently that PTPs such as alkaline phosphatase (ALP) were exploited for the *in situ* generation of pericellular hydrogels.[55–57] Nevertheless, no PTP-triggered targeted drug delivery system has been developed to our best knowledge.

We report in the present work the synthesis of a high drug-loading (44%) Pt(IV)-backboned cationic polymer with excellent aqueous solubility, namely poly(diamminedichlorodisuccinatoplatinum(IV)-diamineethylpiperazine) (P(DSP-DAEP), Fig. 1). P(DSP-DAEP) is more sensitive to reductive activation and shows enhanced *in vitro* anticancer activity compared to its precursor diamminedichlorodisuccinatoplatinum(IV) (DSP). Moreover, P(DSP-DAEP), due to its cationic nature, can form a PEG-shelled polyion complex (Pt-PIC) with an anionic methoxyl poly(ethylene glycol)-*block*-poly(phosphotyrosine) diblock copolymer (mPEG-*b*-PpY) (Fig. 1). Pt-PIC is designed to achieve selective internalization of P(DSP-DAEP) in ALP-overexpressing cancer cells through enzymatic cleavage of the phosphate group of PEG-*b*-PpY,[58] which weakens the polyion complex and consequently accelerates the release of P(DSP-DAEP). In cells without surface ALP, Pt-PIC displays much less internalization due to the PEG-shelled polyion and negative zeta-potential. Thus, this work may provide a new approach to the cell-selective delivery of Pt(IV)-backboned prodrugs *via* phosphatase-responsiveness.

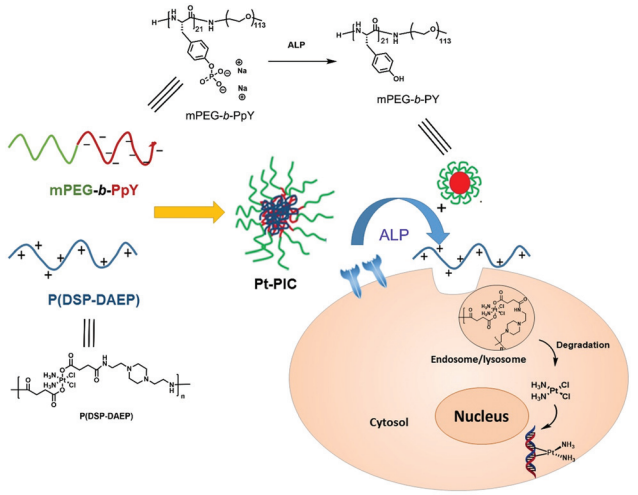


**Fig. 1** Chemical structure of mPEG-*b*-PpY and P(DSP-DAEP), and cartoon illustration of the phosphatase-triggered dissociation of the polyion complex (Pt-PIC).

## Results and discussion

### Synthesis and characterization of P(DSP-DAEP)

To produce a high drug loading and yet a highly water soluble Pt(IV)-backboned polymer, we designed and synthesized the cationic polymer P(DSP-DAEP) as shown in Scheme 1. Briefly, the bis(carboxylic acid)-functionalized Pt(IV) intermediate DSP (Fig. S1 and S2†) was synthesized in two steps by following a previously reported protocol,[39] which was then converted to Pt-NHS, the *N*-hydroxysuccinimide ester form of DSP, by EDC activation in anhydrous DMF.[59] Different from the Shen's protocol in which DSP was directly coupled to bisamines in the presence of EDC, Pt-NHS was synthesized here because it could be purified by a reversed phase C18 column and lyophilized to afford a white powder with high purity (confirmed by $^{1}$H NMR, $^{13}$C NMR and HRESI-MS, Fig. S3–S5†). This purification step was essential to obtain a high-molecular-weight polymer *via* step-growth condensation polymerization. Coupling of Pt-NHS with the bis(primary amine)-functionalized DAEP with strictly equal stoichiometry for 48 h yielded the Pt(IV)-backboned polymer P(DSP-DAEP) in high yield. Thanks to the cationic nature of P(DSP-DAEP), the polymer was highly water soluble without aggregation and could be

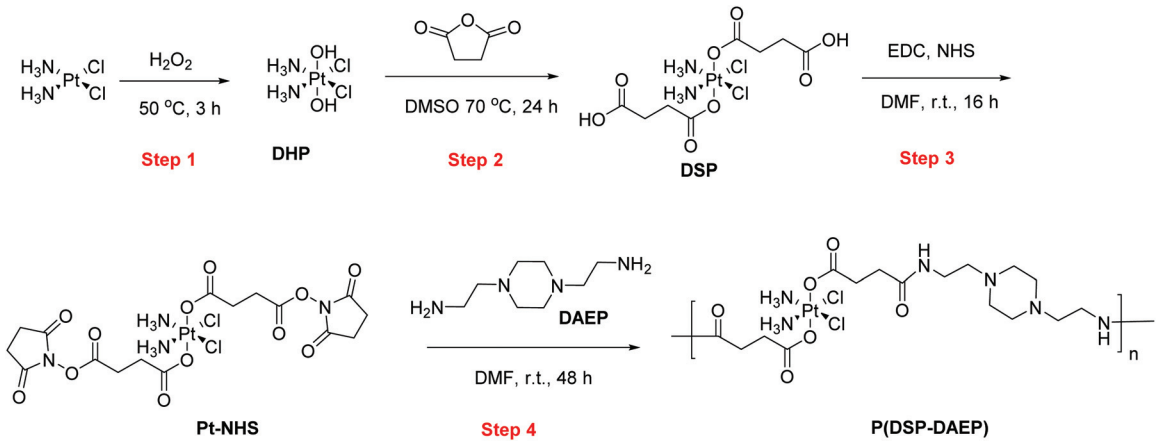


**Scheme 1** Synthesis of P(DSP-DAEP).

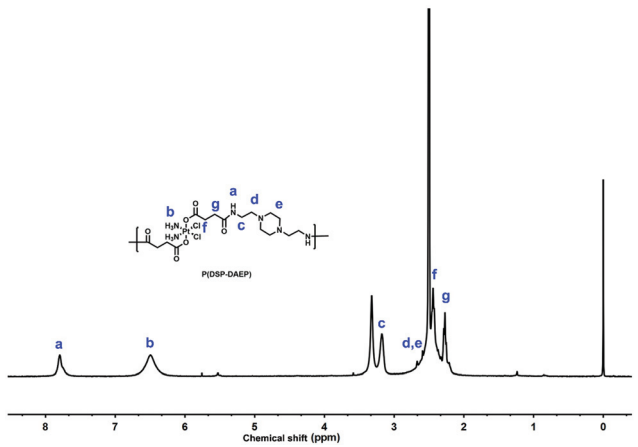


Fig. 2 $^{1}$H NMR spectrum of P(DSP-DAEP) in DMSO-$d_6$.

easily purified by dialysis against ultrapure water. Gel permeation chromatography (GPC) examination of P(DSP-DAEP) revealed a MW of 55.9 kDa and a polydispersity index (PDI) of 2.12 (Fig. S6†). The purity and identity of the polymer was well characterized by $^{1}$H NMR spectroscopy in both DMSO-$d_6$ (Fig. 2) and $D_2O$ (Fig. S7†). The peak at 7.80 ppm was attributable to the newly produced amide proton. The broad peak at 6.50 ppm was attributed to the protons of $NH_3$ derived from the CDDP building block. The purity of P(DSP-DAEP) was further confirmed by its Pt content determined by ICP-MS, which was 29.4% and in good agreement with the theoretical value of 29.1%. This, in turn, gave a drug loading as high as 44.5%.

### Reduction of P(DSP-DAEP)

To examine the degradation of P(DSP-DAEP),[25] the reductive kinetics of DSP and P(DSP-DAEP) were separately monitored by $^{1}$H NMR spectroscopy in a 20 mM ascorbic acid (AsA) solution at 37 °C (Scheme S2 and Fig. S9 and 10†). As shown in Fig. 3a, the polymeric prodrug P(DSP-DAEP) exhibited a faster degradation profile than the small-molecular prodrug DSP. The reductive propensity of the polymer was further evaluated by cyclic voltammetry (CV) at pH 7.4 and 6.0, respectively (Fig. 3b and c).[60] Briefly, the electrochemical studies revealed behaviors characteristic of irreversible reduction of the Pt(IV) axial ligands.[14,61] The reduction potentials were determined by extrapolating to a 0.0 mV s$^{-1}$ scan rate[60] (Fig. S11 and 12†). The reductive potential of P(DSP-DAEP) was determined as −126 and −57 mV at pH 7.4 and 6.0, respectively. This result indicated that P(DSP-DAEP) might be more susceptible to degradation at the slightly acidic tumor microenvironment and in the lysosomes as compared to under normal physiological conditions, which is desirable for an improved therapeutic index.[62] Notably, the reductive potential of DSP, measured by exactly the same method, was reported as −660 and −640 mV at pH 7.4 and 6.0, respectively,[39] which further confirmed that the polymeric P(DSP-DAEP) was more sensitive to the reductive environment compared to DSP. The higher sensitivity to the reduction of P(DSP-DAEP) may be attributed to its bulkiness as a polymer as compared to DSP as a small molecule.[63]

### *In vitro* cytotoxicity of P(DSP-DAEP)

The cytotoxicities of DSP and P(DSP-DAEP) were evaluated in A549 (human lung cancer), HeLa (human cervical cancer), U-2OS (human osteosarcoma) and Saos-2 (human osteosarcoma) cancer cells by using CellTiter Blue assays. Interestingly, P(DSP-DAEP) demonstrated significant or slightly higher potency than its precursor DSP in all the cell lines tested. For example, the $IC_{50}$ values of P(DSP-DAEP) in A549 and HeLa cells were determined as 62 and 79 μM, respectively; in comparison, the numbers for DSP in the same cell lines were $3.6 \times 10^2$ and $3.1 \times 10^2$ μM, respectively (Table 1 and Fig. S13†). Thus, the polymer was ~4–6 fold more potent than the small-molecular DSP in these two cells. Similarly, in U-2OS and Saos-2 cells, the $IC_{50}$ values of P(DSP-DAEP) were also slightly smaller than DSP (Table 1 and Fig. S13†). It is worth pointing out that the cellular uptake rate of DSP and P(DSP-DAEP) was comparable (Fig. S14†); moreover, when the cells were treated with DAEP, no cytotoxicity was observed up to 1.5 mM (Fig. S15†). Overall, the higher potency of P(DSP-DAEP)

Table 1 *In vitro* $IC_{50}$ values of DSP and P(DSP-DAEP) in various cancer cells

| $IC_{50}$ (μM) | A549 | HeLa | U-2OS | Saos-2 |
|---|---|---|---|---|
| DSP | 360 | 309 | 72 | 281 |
| P(DSP-DAEP) | 62 | 79 | 63 | 167 |

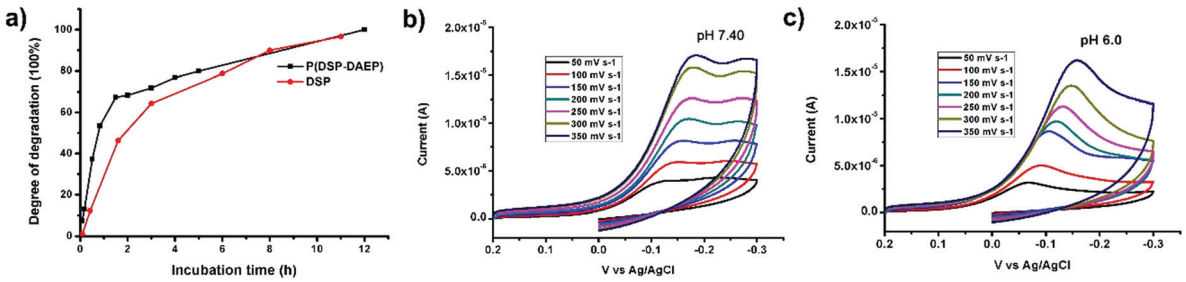


Fig. 3 (a) Degradation profiles of P(DSP-DAEP) and DSP with the addition of ascorbic acid (4.0 eq., 20 mM) at 37 °C, pH 7.4. (b and c) Cyclic voltammograms of P(DSP-DAEP) in PBS–0.1 M KCl with varied scan rates at pH 7.4 (b) and 6.0 (c).

 

compared to DSP was in good agreement with the results of previous reduction experiments (Fig. 3).

### Pt-PIC formation and ALP-responsiveness

To impart targeting modality and further expand the therapeutic window, we generated Pt-PIC by simply mixing the cationic P(DSP-DAEP) with an anionic ALP-responsive polypeptide mPEG-*b*-PpY (Fig. S16†). Depending on the P/Pt molar ratio (1/1–3/1), the drug loading of Pt-PIC varied between 13 and 21% (Table S1†). We fixed the P/Pt ratio to 2/1 in our subsequent studies. To test the ALP-responsiveness of Pt-PIC, an aliquot of ALP was added to the polyion complex and the mixture was incubated at 37 °C for 12 h. $^{31}$P NMR spectroscopy depicted an ~70% dephosphorylation of Pt-PIC within 1 hour as shown in Fig. 4a and S17.† Dynamic light scattering measurement showed that the hydrodynamic volume of Pt-PIC shrank dramatically from ~178 to ~56 nm after ALP treatment (Fig. 4b and Table S2†). The reduced size of ALP-treated Pt-PIC could be attributed to the resultant poly(L-tyrosine) core, which was more compact than the polyion complex in Pt-PIC. Moreover, the zeta-potential of Pt-PIC increased from −71 to −29 mV after enzyme treatment, likely due to the dephosphorylation process (Fig. 4c and Table S2†). Interestingly, ALP-treated mPEG-*b*-PpY showed a size of 62 nm and a zeta potential of −36 mV, which were comparable to those of ALP-treated Pt-PIC (Fig. 4b and c). This coincidence implied that ALP-treated Pt-PIC might form particles composed of poly(ethylene glycol)-*block*-poly(L-tyrosine), the same product of ALP-treated mPEG-*b*-PpY.[64,65] Notably, the formation of Pt-PIC did not affect the reduction of P(DSP-DAEP) as determined by ICP-MS (Fig. 4d). Taken together, the results suggested that ALP could enzymatically cleave the phosphate group of mPEG-*b*-PpY, which subsequently led to the disruption of Pt-PIC and release of P(DSP-DAEP) because of the weakened electrostatic interactions.

### CLSM study in ALP$^{+/-}$ cells

To confirm the ALP-responsiveness of Pt-PIC at the cellular level, confocal laser scanning microscopy (CLSM) was used to monitor the internalization of FAM-labeled P(DSP-DAEP) and Pt-PIC by using Saos-2 (ALP positive) and U-2OS (ALP negative) cell lines (Fig. S18†). As positively charged polymers and nanoparticles have been previously reported to show effective cell uptake,[18,66] FAM-labeled P(DSP-DAEP) was indeed readily taken up by both cell lines after 3 h of incubation at 37 °C (Fig. 5). An overlay of the LysoTracker Red channel and FAM channel revealed that the polymer was mainly localized in the lysosomes, in which the Pt(IV) polymer might be easily and rapidly reduced to release active Pt(II) due to the slightly acidic pH value. Interestingly, Pt-PIC was internalized into the ALP$^{+}$ Saos-2 cells with a similar level compared to the naked P(DSP-DAEP), whereas no observable polymer fluorescence was detected in the Pt-PIC treated ALP$^{-}$ U-2OS cells. The dramatic difference in the internalization pattern of Pt-PIC in Saos-2 and U-2OS cells was provisionally attributed to the dephosphorylation of mPEG-*b*-PpY by the ectoenzyme ALP,

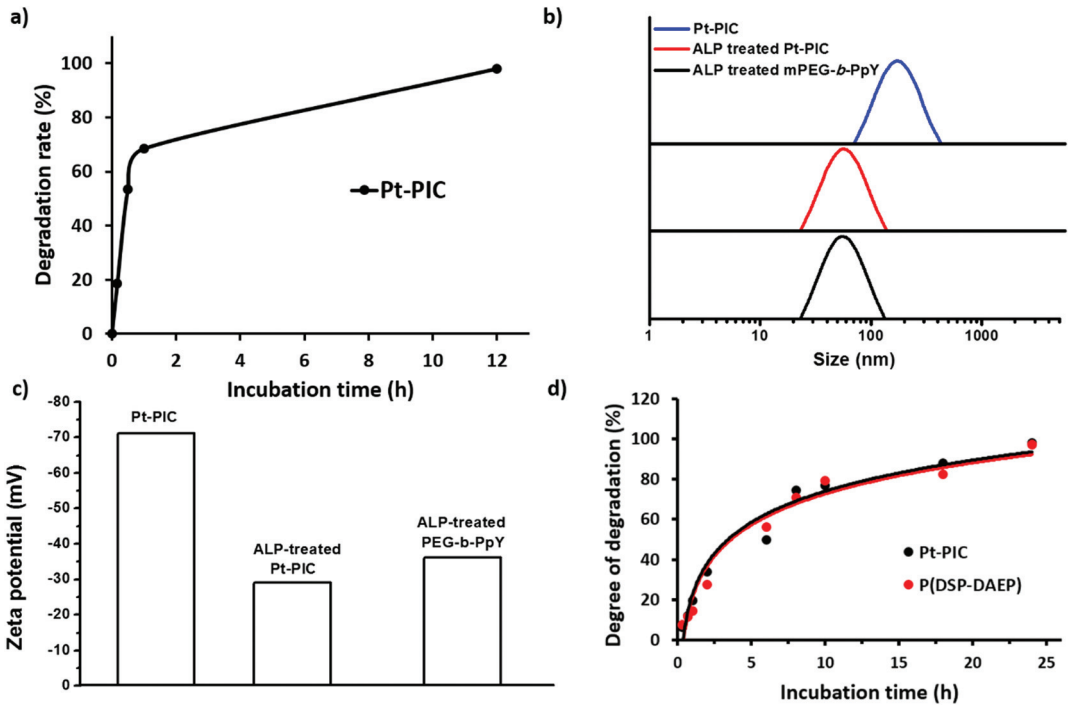


**Fig. 4** (a) Dephosphorylation profile of ALP-treated Pt-PIC at 37 °C, pH 8.0; determined by $^{31}$P NMR. (b) DLS and (c) zeta potential measurement of Pt-PIC, ALP-treated Pt-PIC and ALP-treated mPEG-*b*-PpY. (d) Pt release profile of Pt-PIC and P(DSP-DAEP) with the addition of ascorbic acid (5.0 eq., 5.0 mM) at 25 °C, pH 7.4.

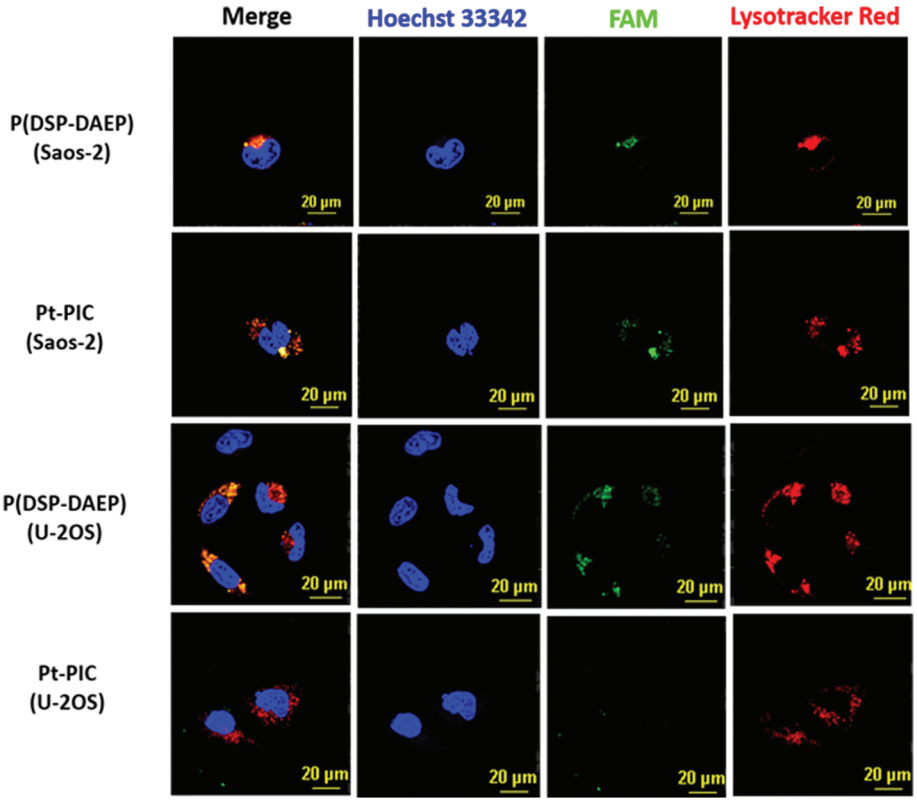


Fig. 5 Confocal laser scanning microscopy analysis of the uptake of P(DSP-DAEP) and Pt-PIC in Saos-2 (ALP positive) and U-2OS (ALP negative) cells. The cells were separately treated with each material at 5 μM platinum for 3 h.

which was overexpressed on the cell surface of Saos-2 cells, but not on U-2OS cells.

### Cell selective toxicity of Pt-PIC

To further evaluate the ALP-dependence of Pt-PIC and its improved therapeutic window, one should test, compared to the naked P(DSP-DAEP), whether Pt-PIC could show different cytotoxicity according to the ALP levels of cells. For this, we again incubated Saos-2 and U-2OS cells with P(DSP-DAEP) and Pt-PIC at various concentrations separately. Since mPEG-*b*-PpY did not show any sign of toxicity to both cells at concentrations as high as 2.8 mg $mL^{-1}$ (Fig. S19†), the toxicity of Pt-PIC must be exclusively derived from P(DSP-DAEP). As shown in Fig. 6, the *Y* axis represents the relative cytotoxicity of Pt-PIC normalized to that of P(DSP-DAEP) at a certain concentration. In the $ALP^-$ U-2OS cells, the relative cytotoxicity of Pt-PIC to P(DSP-DAEP) was decreased by almost two fold at all the concentrations tested (triangle legend (△), Fig. 6). This was perhaps due to the impeded internalization of Pt-PIC in the U-2OS cells as we previously observed in the CLSM study (Fig. 5). In comparison, the anti-cancer toxicity of Pt-PIC showed no difference with P(DSP-DAEP) in the $ALP^+$ Saos-2 cells (dot legend (●), Fig. 6), which indicated that Pt-PIC could effectively deliver the polymeric Pt(IV)-prodrug to Saos-2 cells at the same level as the naked P(DSP-DAEP) did. Altogether, the

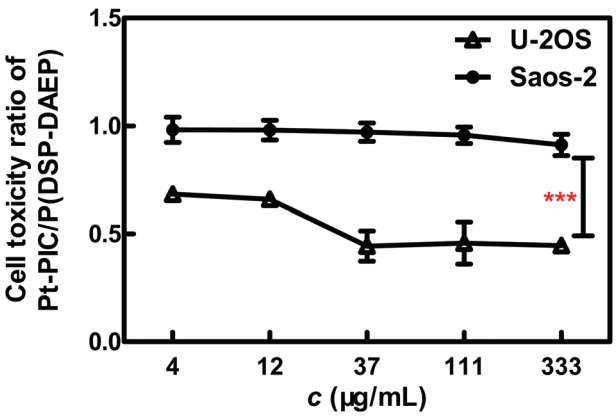


Fig. 6 Relative cytotoxicity ratio of Pt-PIC/P(DSP-DAEP) in Saos-2 (ALP positive) and U-2OS (ALP negative) cells.

results implied that Pt-PIC could improve the therapeutic index of P(DSP-DAEP) by selectively targeting $ALP^+$ cells.

## Conclusions

In conclusion, we have designed and synthesized a positively-charged prodrug P(DSP-DAEP) with Pt(IV) embedded in the

 

backbone. P(DSP-DAEP), with a high and constant drug loading content, could be rapidly reduced in a reductive environment to release the active cisplatin. As a prodrug, P(DSP-DAEP) showed higher potency than its small molecular precursor DSP. Moreover, the cationic P(DSP-DAEP) could form a polyion complex with the anionic mPEG-*b*-PpY *via* polyelectrolyte coacervation. Preliminary *in vitro* cellular uptake and cytotoxicity assay suggested that Pt-PIC exhibited cell selective internalization and toxicity depending on their ectoenzyme ALP expression levels. Overall, our data suggested a new strategy for the cell-selective delivery of platinum-based anticancer drugs.

## Experimental section

### Materials

All chemicals were purchased from commercial sources and used as received unless otherwise specified. *cis*-Diamminedichloroplatinum(II) (cisplatin, CDDP) was purchased from HWRK Chem Co., Ltd (Beijing, China). Methoxypolyethylene glycol amine (mPEG-$NH_2$, MW = 5000 Da) was purchased from Aladdin Industrial Corporation (China). 5-Carboxyfluorescein *N*-hydroxysuccinimide ester (5-FAM SE) was purchased from OKeanos Tech. Co., Ltd (Beijing, China). Anhydrous *N*,*N*-dimethylformamide (DMF) was purchased from Sigma-Aldrich. Calf intestinal alkaline phosphatase (10 000 U $mL^{-1}$) was purchased from New England Biolabs Inc.

### Instrumentation

NMR spectra were recorded on a 400 MHz Bruker ARX400 FT-NMR spectrometer. Fourier transform infrared (FT-IR) spectra were recorded on a Bruker Vector 22 FT-IR spectrometer and quantification was realized by using a KBr cell with a fixed path length of 0.2 mm. Inductively Coupled Plasma Mass Spectrometry (ICP-MS) was performed on a NexION 350X (PerkinElmer, USA). Dynamic light scattering and zeta potential were measured at 25 °C on a Nanobrook Omni (Brookhaven Instrument Corp. New York, USA), with a laser operating at 640 nm. Analyses were performed at an angle of 90° collecting optics. Tandem gel permeation chromatography (GPC) experiments were performed on a system equipped with an isocratic pump (Model 1100, Agilent Technology, Santa Clara, CA), and an Optilab rEX refractive index detector (Wyatt Technology, Santa Barbara, CA). The temperature of the refractive index detectors was 25 °C. Separations were performed using serially connected size exclusion columns (500, $10^3$, $10^4$, and $10^5$ Å Phenogel columns, 5 μm, 7.8 × 300 mm, Phenomenex, Torrance, CA) at 50 °C using DMF containing 0.1 M LiBr as the mobile phase. Polystyrene standards were used to generate a calibration curve. Cyclic Voltammetry (CV) was performed on a BASi Epsilon workstation. Confocal images were taken on a Nikon A1R confocal laser scanning microscope system attached to an inverted ECLIPSE Ti (Nikon Corp., Japan). The flow cytometry analysis was performed on a BD LSR Fortessa equipped with 405, 488 and 640 nm lasers (BD Biosciences, USA). Cytotoxicity studies were assayed with an EnSpire® Multimode Plate Reader (PerkinElmer, USA).

### Synthesis

DHP, DSP,[13,67] DAEP[68] and Pt-NHS[59,69] (Scheme 1) were synthesized by following previously reported protocols with minor modification. PEG-*b*-PpY was prepared based on our previous work[58] and confirmed by $^1$H NMR.

**Synthesis of DHP.** Cisplatin (1.0 g, 3.34 mmol) was suspended in 25 mL of DI water, to which was added $H_2O_2$ (35 mL, 30% in water). The mixture was heated to 50 °C and stirred for 3 h in the dark, and then allowed to cool to room temperature, followed by further cooling down to 0 °C in an ice/water bath. The solid was collected by filtration, rinsed with cold water, ethanol, and ether. The product was dried under vacuum to give a yellow solid (830 mg, yield 74%).

**Synthesis of DSP.** To a solution of DHP (415 mg, 1.24 mmol) in DMSO (6.0 mL) was added succinic anhydride (497 mg, 4.97 mmol), and the reaction mixture was heated to 70 °C and stirred for 24 h in the dark. The solvent was removed by lyophilization, and the residue was suspended in acetone (10 mL), precipitated with ether (50 mL), filtered and washed with ether (30 mL). The resulting solid was re-suspended in acetone again (5 mL), sonicated, precipitated with ether (40 mL), filtered, and dried under high vacuum to afford a light yellow solid (520 mg, yield 78%). $^1$H NMR (400 MHz, DMSO-$d_6$) $\delta$ 12.09 (s, 2H), 6.49 (s, 6H), 2.48 (s, 4H), 2.37 (t, $J$ = 7.0 Hz, 4H).

**Synthesis of Pt-NHS.** DSP (322 mg, 0.60 mmol) was dissolved in anhydrous DMF (5 mL), to which were added *N*-(3-dimethylaminopropyl)-*N*′-ethylcarbodiimide hydrochloride (EDC, 242 mg, 1.26 mmol) and *N*-hydroxysuccinimide (NHS, 145 mg, 1.26 mmol). The reaction mixture was stirred at room temperature for 16 h in the dark. Afterward, the reaction mixture was purified by an automatic chromatography system equipped with a reverse phase C18 column (solvent A: water with 0.1% TFA, solvent B: $CH_3CN$; elution conditions: 5% B for 10 min, 5% to 50% B for 25 min). The pure fractions were quickly collected and lyophilized directly to yield the desired product as a white solid (327 mg, 75%). $^1$H NMR (400 MHz, DMSO-$d_6$) $\delta$ 6.49 (br s, 6H), 2.86–2.76 (m, 12H), 2.64 (t, $J$ = 6.9 Hz, 4H). $^{13}$C NMR (101 MHz, DMSO-$d_6$) $\delta$ 178.6, 170.7, 168.9, 30.0, 27.2, 25.9. HRMS (ESI): $m/z$ $[M + H]^+$ calcd 728.03320, found 728.03144, error 2.4 ppm; $[M + NH_4]^+$ calcd 745.05974, found 745.05929, error 0.8 ppm.

**Synthesis of polymer P(DSP-DAEP).** A 5 mL vial was charged with Pt-NHS (291.2 mg, 0.4 mmol) and 2,2′-(piperazine-1,4-diyl)bis(ethan-1-amine) DAEP (69.0 mg, 0.40 mmol), followed by anhydrous DMF (1.2 mL). The vial was flushed with nitrogen and stirred at room temperature for 48 h in the dark. The crude product was precipitated in methanol (40 mL), washed with methanol (40 mL, twice) and ether (40 mL, twice), and dried under high vacuum. The resulting solid was further purified by dialysis against DI water (MWCO 1000 Da) at 4 °C in the dark for 12 h before lyophilization to give a light gray solid (183 mg, 68% yield).

$^1$H NMR (400 MHz, $D_2O$) $\delta$ 3.44 (s), 2.92–2.81 (m), 2.71–2.66 (m), 2.53–2.47 (m). $^1$H NMR (400 MHz, DMSO-$d_6$) $\delta$ 7.80 (br s), 6.50 (br s), 3.18 (br s), 2.67–2.35 (m), 2.29–2.21 (m). Elemental analysis by ICP-AES: Pt (wt%) calc. 29.4%; obtained 29.1%.

**Synthesis of FAM-P(DSP-DAEP).** A 5 mL vial was charged with Pt-NHS (145.6 mg, 0.20 mmol) and 2,2′-(piperazine-1,4-diyl)bis(ethan-1-amine) DAEP (34.5 mg, 0.20 mmol), followed by anhydrous DMF (1.2 mL). The vial was flushed with nitrogen and stirred at room temperature for 48 h in the dark. Then an additional aliquot of DAEP (3.4 mg, 0.02 mmol, 0.10 eq.) was added and stirred at r.t. for 24 h to ensure an amine-ended polymer. The resulting polymer was continuously conjugated to 5-FAM-SE (14.2 mg, 0.03 mmol, 0.20 eq.) and stirred for another 24 h. The crude product was precipitated in methanol (40 mL), washed with methanol (40 mL, twice) and ether (40 mL, twice), and dried under high vacuum. The crude product was further purified by dialysis against DI water (MWCO 1000 Da) at 4 °C in the dark for 12 h before lyophilization to give an orange solid (56 mg).

### Electrochemistry

Cyclic Voltammetry (CV) was performed by using degassed phosphate-buffer (10 mM, pH 6.0 or 7.4) with 0.1 M KCl as the supporting electrolyte. The glassy carbon electrode and platinum wire was used as the working electrode and counter electrode, respectively. All potentials were represented using Ag/AgCl (saturated) as the reference electrode. The platinum concentration of the polymer was set at 1.0 mM at varying scan rates between 50 and 350 mV $s^{-1}$. The electrolyte solution was bubbled with nitrogen for 20 minutes before each measurement.

### Reductive degradation of P(DSP-DAEP)

The reductive degradation of P(DSP-DAEP) was quantitatively monitored by $^1$H NMR spectroscopy. Briefly, P(DSP-DAEP) (1.7 mg, 5.0 mmol Pt, 1.0 eq.) was incubated with ascorbic acid (4.0 eq.) in 2× PBS of $D_2O$ (0.50 mL, pH 7.4) at 37 °C. $^1$H NMR spectra were recorded at various time points. The quantification was realized by monitoring the disappearance of the methylene peak at $\delta$ 2.68 ppm (peak of the proton $a_1$) and the appearance of a peak at $\delta$ 2.48 ppm (peak of the proton $a_2$) (Scheme S2 and Fig. S10†).

### Polyion complex (PIC) preparation and phosphatase-responsiveness

Pt-PIC was prepared by adding the PEG-*b*-PpY solution (20 mM, 60 μL) into P(DSP-DAEP) (20 mM, 30 μL) in ultrapure water. The mixture was then diluted to 1.2 mL with ultrapure water to give a final concentration of 0.5 mM Pt(IV). To examine the phosphatase-responsiveness, the pH of the PICs was carefully adjusted to slightly basic by 0.1 N NaOH (pH 7.4–8.6) and the resulting complexes were incubated at room temperature for 30 min before the assay. Alkaline phosphatase (ALP, 10 U $\mu L^{-1}$, 4 μL) was added to the PICs (1.0 mL) and incubated at 37 °C for 12 hours. The mixture was characterized by DLS and zeta potential.

### Reductive properties of P(DSP-DAEP) and Pt-PIC measured by ICP-MS

1.0 mL of Pt-PIC or P(DSP-DAEP) (Pt content 1.0 mM) was separately placed into a pre-swelled dialysis bag (cutoff molecular weight of 1.0 kDa) and immersed into 99 mL of 50 mM Tris·HCl buffer (pH = 7.4) containing 5.0 mM ascorbic acid. The Pt-PIC was dialyzed in a shaking culture incubator at 25 °C. 1.0 mL of sample was withdrawn from the medium outside the dialysis bag at specified time intervals, which was measured for the Pt content by ICP-MS.

### Dephosphorylation process of Pt-PIC with ALP measured by $^{31}$P NMR

To a Pt-PIC (~10 mg PpY) solution in 100 mM Tris·DCl buffer (pH = 8.0, 0.50 mL $D_2O$), was added ALP (10 U $\mu L^{-1}$ × 4 μL). The mixture was incubated at 37 °C and measured by $^{31}$P NMR at intervals.

### Cell culture

Human osteosarcoma cell lines Saos-2 and U-2OS were obtained from Prof. Shuyan Li (Peking University). A549 and HeLa were obtained as generous gifts from Prof. Shu Wang (Institute of Chemistry Chinese Academy of Sciences) and Prof. Peng R. Chen (Peking University) respectively. The Saos-2 and U-2OS cells were cultured in DMEM (Corning, Manassas, USA) supplemented with 10% FBS (Gibco), 100 U $mL^{-1}$ penicillin and 100 U $mL^{-1}$ streptomycin (Corning, Manassas, USA) under a humidified atmosphere containing 5% $CO_2$ at 37 °C.

### *In vitro* cell uptake of DSP and P(DSP-DAEP)

5 × $10^6$ HeLa cells were seeded in Corning® 100 mm TC-treated culture dishes and incubated for 24 h before experiments. The cells were treated with DSP or P(DSP-DAEP) at 37 °C for 3 h. The cells were washed with 1× PBS, heparin (1 mg $mL^{-1}$) and 1× PBS, trypsinized and cell numbers were counted. The cells were then digested by $HNO_3$ and the intracellular Pt amount was measured by ICP-MS.

### Flow cytometry assay

The ALP expression level of Saos-2 and U-2OS was confirmed by flow cytometry assay with a mouse PE-labeled anti-human ALP monoclonal antibody (BD Biosciences, USA) following the manufacturer's protocol. Briefly, the Saos-2 and U-2OS cells were grown in a T75 $cm^2$ flask to 90% confluence and detached by a cell stripper (2 mL, Corning). The cells (~1.0 × $10^5$ cells) were resuspended and incubated on ice in a PBS buffer (pH 7.4, 50 μL) supplemented with 3% BSA and 1 μL anti-ALP antibody for 30 min in the dark. The stained cells were rinsed with PBS (500 μL) 3 times and suspended in cold PBS for flow cytometry analysis.

### Confocal laser scanning microscopy analysis

The Saos-2/U-2OS cells in the exponential growth phase were seeded in glass bottomed culture chambers (20 mm, Nest) at a density of 1 × $10^5$ cells per well. The cells were incubated at

 

37 °C under a humidified atmosphere containing 5% $CO_2$ for 24 h. The cells were treated with fresh medium (1.0 mL) containing FAM-labeled P(DSP-DAEP) and Pt-PIC (5 μM based on platinum) for 3 h. The cells were washed with 1× PBS (1 mL × 3) and stained with Hoechst 33342 (Life Technologies Inc. Carlsbad, USA) and LysoTracker® Red (Life Technologies Inc. Carlsbad, USA) for 20 min at 37 °C in the dark. The cells were imaged in cell culture medium (1.0 mL) after repetitive rinsing with 1× PBS (1.0 mL) three times. FAM-labeled P(DSP-DAEP) was prepared by conjugating 5-FAM-SE to amine-capped P(DSP-DAEP), which was obtained by maintaining a slightly higher stoichiometry of DAEP during the step-growth polymerization. The FAM-labeled polymer was purified by dialysis against water (MW 3500) and lyophilized to afford an orange solid.

### Cell viability assay

The Saos-2/U-2OS cells in the exponential growth phase were seeded into a black 96-well plate at a density of 5000 cells per well 24 h prior to the assay. The culture medium was removed and the cells were treated with DSP, P(DSP-DAEP), or Pt-PIC in fresh medium at gradient concentrations ($n$ = 3). After incubation for a certain time, the relative cell viabilities were monitored by the CellTiter-Blue® cell viability assay (Promega, USA) following the manufacturer's protocol. The $IC_{50}$ values were calculated by using GraphPad Prism version 5 using log(inhibitor) *vs.* the response regression method.

## Acknowledgements

This work was financially supported by the National Key Research and Development Program of China (no. 2016YFA0201400). H. L. thanks the grants from the National Natural Science Foundation of China (NSFC21434008), and the Open Funding Project of the State Key Laboratory of Biochemical Engineering (no. 2015KF-01). S.-L. was supported in part by the China Postdoctoral Science Foundation (no. 2016 M600847) and the Postdoctoral Fellowship of the Peking-Tsinghua Center for Life Sciences.

## References

1 L. Kelland, *Nat. Rev. Cancer*, 2007, **7**, 573–584.
2 N. Nishiyama, S. Okazaki, H. Cabral, M. Miyamoto, Y. Kato, Y. Sugiyama, K. Nishio, Y. Matsumura and K. Kataoka, *Cancer Res.*, 2003, **63**, 8977–8983.
3 H. Cabral, Y. Matsumoto, K. Mizuno, Q. Chen, M. Murakami, M. Kimura, Y. Terada, M. R. Kano, K. Miyazono, M. Uesaka, N. Nishiyama and K. Kataoka, *Nat. Nanotechnol.*, 2011, **6**, 815–823.
4 S. Guo, Y. Wang, L. Miao, Z. Xu, C. M. Lin, Y. Zhang and L. Huang, *ACS Nano*, 2013, **7**, 9896–9904.
5 X. Xue, M. D. Hall, Q. Zhang, P. C. Wang, M. M. Gottesman and X. J. Liang, *ACS Nano*, 2013, **7**, 10452–10464.
6 M. Callari, J. R. Aldrich-Wright, P. L. de Souza and M. H. Stenzel, *Prog. Polym. Sci.*, 2014, **39**, 1614–1643.
7 L. Miao, S. Guo, J. Zhang, W. Y. Kim and L. Huang, *Adv. Funct. Mater.*, 2014, **24**, 6601–6611.
8 S. Shen, C. Y. Sun, X. J. Du, H. J. Li, Y. Liu, J. X. Xia, Y. H. Zhu and J. Wang, *Biomaterials*, 2015, **70**, 71–83.
9 H. Y. Yu, Z. H. Tang, D. W. Zhang, W. T. Song, Y. Zhanga, Y. Yang, Z. Ahmad and X. S. Chen, *J. Controlled Release*, 2015, **205**, 89–97.
10 S. Kaur, C. Prasad, B. Balakrishnan and R. Banerjee, *Biomater. Sci.*, 2015, **3**, 955–987.
11 J. Kim, S. Pramanick, D. Lee, H. Park and W. J. Kim, *Biomater. Sci.*, 2015, **3**, 1002–1017.
12 S. Dhar, F. X. Gu, R. Langer, O. C. Farokhzad and S. J. Lippard, *Proc. Natl. Acad. Sci. U. S. A.*, 2008, **105**, 17356–17361.
13 W. J. Rieter, K. M. Pott, K. M. L. Taylor and W. B. Lin, *J. Am. Chem. Soc.*, 2008, **130**, 11584–11585.
14 S. Dhar, W. L. Daniel, D. A. Giljohann, C. A. Mirkin and S. J. Lippard, *J. Am. Chem. Soc.*, 2009, **131**, 14652–14653.
15 S. Venkataraman, J. L. Hedrick, Z. Y. Ong, C. Yang, P. L. R. Ee, P. T. Hammond and Y. Y. Yang, *Adv. Drug Delivery Rev.*, 2011, **63**, 1228–1246.
16 H. Q. Song, H. H. Xiao, Y. Zhang, H. D. Cai, R. Wang, Y. H. Zheng, Y. B. Huang, Y. X. Li, Z. G. Xie, T. J. Liu and X. B. Jing, *J. Mater. Chem. B*, 2013, **1**, 762–772.
17 R. K. Pathak, S. Marrache, J. H. Choi, T. B. Berding and S. Dhar, *Angew. Chem., Int. Ed.*, 2014, **53**, 1963–1967.
18 N. Bertrand, J. Wu, X. Xu, N. Kamaly and O. C. Farokhzad, *Adv. Drug Delivery Rev.*, 2014, **66**, 2–25.
19 Y.-R. Zheng, K. Suntharalingam, T. C. Johnstone, H. Yoo, W. Lin, J. G. Brooks and S. J. Lippard, *J. Am. Chem. Soc.*, 2014, **136**, 8790–8798.
20 C. B. He, C. Poon, C. Chan, S. D. Yamada and W. B. Lin, *J. Am. Chem. Soc.*, 2016, **138**, 6010–6019.
21 C.-H. Lin, S.-H. Cheng, W.-N. Liao, P.-R. Wei, P.-J. Sung, C.-F. Weng and C.-H. Lee, *Int. J. Pharm.*, 2012, **429**, 138–147.
22 X. Xu, K. Xie, X. Q. Zhang, E. M. Pridgen, G. Y. Park, D. S. Cui, J. Shi, J. Wu, P. W. Kantoff, S. J. Lippard, R. Langer, G. C. Walker and O. C. Farokhzad, *Proc. Natl. Acad. Sci. U. S. A.*, 2013, **110**, 18638–18643.
23 S. G. Awuah, Y. R. Zheng, P. M. Bruno, M. T. Hemann and S. J. Lippard, *J. Am. Chem. Soc.*, 2015, **137**, 14854–14857.
24 T. C. Johnstone, K. Suntharalingam and S. J. Lippard, *Chem. Rev.*, 2016, **116**, 3436–3486.
25 J. J. Wilson and S. J. Lippard, *Chem. Rev.*, 2014, **114**, 4470–4495.
26 R. K. Pathak and S. Dhar, *Chem. – Eur. J.*, 2016, **22**, 3029–3036.
27 D. Zhou, Y. Cong, Y. Qi, S. He, H. Xiong, Y. Wu, Z. Xie, X. Chen, X. Jing and Y. Huang, *Biomater. Sci.*, 2015, **3**, 182–191.
28 S. Aryal, C.-M. J. Hu and L. Zhang, *ACS Nano*, 2010, **4**, 251–258.

29 Z.-T. Cao, Z.-Y. Chen, C.-Y. Sun, H.-J. Li, H.-X. Wang, Q.-Q. Cheng, Z.-Q. Zuo, J.-L. Wang, Y.-Z. Liu, Y.-C. Wang and J. Wang, *Biomaterials*, 2016, **94**, 9–19.
30 J. D. Rocca, M. E. Werner, S. A. Kramer, R. C. Huxford-Phillips, R. Sukumar, N. D. Cummings, J. L. Vivero-Escoto, A. Z. Wang and W. Lin, *Nanomedicine*, 2015, **11**, 31–38.
31 D. Liu, C. Poon, K. Lu, C. He and W. Lin, *Nat. Commun.*, 2014, **5**, 4182.
32 Q. Yang, J. Cai, S. Sun, X. Kang, J. Guo, Y. Zhu, L. Yan, X. Jing and Z. Wang, *Biomater. Sci.*, 2016, **4**, 661–669.
33 H. Zhou, G. Wang, Y. Lu and Z. Pan, *Biomater. Sci.*, 2016, **4**, 1212–1218.
34 P. Huang, D. Wang, Y. Su, W. Huang, Y. Zhou, D. Cui, X. Zhu and D. Yan, *J. Am. Chem. Soc.*, 2014, **136**, 11748–11756.
35 K. Cai, X. He, Z. Song, Q. Yin, Y. Zhang, F. M. Uckun, C. Jiang and J. Cheng, *J. Am. Chem. Soc.*, 2015, **137**, 3458–3461.
36 H. Tang, C. J. Murphy, B. Zhang, Y. Shen, E. A. Van Kirk, W. J. Murdoch and M. Radosz, *Biomaterials*, 2010, **31**, 7139–7149.
37 Y. Dai, X. Kang, D. Yang, X. Li, X. Zhang, C. Li, Z. Hou, Z. Cheng, P. a. Ma and J. Lin, *Adv. Healthcare Mater.*, 2013, **2**, 562–567.
38 X.-D. Xu, Y.-J. Cheng, J. Wu, H. Cheng, S.-X. Cheng, R.-X. Zhuo and X.-Z. Zhang, *Biomaterials*, 2016, **76**, 238–249.
39 J. Yang, W. W. Liu, M. H. Sui, J. B. Tang and Y. Q. Shen, *Biomaterials*, 2011, **32**, 9136–9143.
40 Z. Cao, R. Tong, A. Mishra, W. Xu, G. C. L. Wong, J. Cheng and Y. Lu, *Angew. Chem., Int. Ed.*, 2009, **121**, 6616–6620.
41 S. Dhar, N. Kolishetti, S. J. Lippard and O. C. Farokhzad, *Proc. Natl. Acad. Sci. U. S. A.*, 2011, **108**, 1850–1855.
42 W. T. Song, M. Q. Li, Z. H. Tang, Q. S. Li, Y. Yang, H. Y. Liu, T. C. Duan, H. Hong and X. S. Chen, *Macromol. Biosci.*, 2012, **12**, 1514–1523.
43 N. Graf, D. R. Bielenberg, N. Kolishetti, C. Muus, J. Banyard, O. C. Farokhzad and S. J. Lippard, *ACS Nano*, 2012, **6**, 4530–4539.
44 J. Della Rocca, R. C. Huxford, E. Comstock-Duggan and W. Lin, *Angew. Chem., Int. Ed.*, 2011, **123**, 10514–10518.
45 S. Guo, C. M. Lin, Z. Xu, L. Miao, Y. Wang and L. Huang, *ACS Nano*, 2014, **8**, 4996–5009.
46 M. Patra, T. C. Johnstone, K. Suntharalingam and S. J. Lippard, *Angew. Chem., Int. Ed.*, 2016, **55**, 2550–2554.
47 L. Zhu, P. Kate and V. P. Torchilin, *ACS Nano*, 2012, **6**, 3491–3498.
48 J. Li, Z. Ge and S. Liu, *Chem. Commun.*, 2013, **49**, 6974–6976.
49 L. Zhu, T. Wang, F. Perche, A. Taigind and V. P. Torchilin, *Proc. Natl. Acad. Sci. U. S. A.*, 2013, **110**, 17047–17052.
50 Y. Liu, D. Zhang, Z. Y. Qiao, G. B. Qi, X. J. Liang, X. G. Chen and H. Wang, *Adv. Mater.*, 2015, **27**, 5034–5042.
51 H. Li, J. Du, X. Du, C. Xu, C. Sun, H. Wang, Z. Cao, X. Yang, Y. Zhu, S. Nie and J. Wang, *Proc. Natl. Acad. Sci. U. S. A.*, 2016, **113**, 4164–4169.
52 R. Mo, T. Jiang, R. Disanto, W. Tai and Z. Gu, *Nat. Commun.*, 2014, **5**, 3364–3364.
53 A. Ostman, C. Hellberg and F. D. Böhmer, *Nat. Rev. Cancer*, 2006, **6**, 307–320.
54 V. V. Vintonyak, A. P. Antonchick, D. Rauh and H. Waldmann, *Curr. Opin. Chem. Biol.*, 2009, **13**, 272–283.
55 J. Zhou, X. Du, N. Yamagata and B. Xu, *J. Am. Chem. Soc.*, 2016, **138**, 3813–3823.
56 R. A. Pires, Y. M. Abul-Haija, D. S. Costa, R. Novoa-Carballal, R. L. Reis, R. V. Ulijn and I. Pashkuleva, *J. Am. Chem. Soc.*, 2015, **137**, 576–579.
57 Y. Kuang, J. Shi, J. Li, D. Yuan, K. A. Alberti, Q. Xu and B. Xu, *Angew. Chem., Int. Ed.*, 2014, **126**, 8242–8245.
58 Y. Sun, Y. Hou, X. Zhou, J. Yuan, J. Wang and H. Lu, *ACS Macro Lett.*, 2015, **4**, 1000–1003.
59 Y. Yuan, R. T. K. Kwok, B. Z. Tang and B. Liu, *J. Am. Chem. Soc.*, 2014, **136**, 2546–2554.
60 R. S. Nicholson and I. Shain, *Anal. Chem.*, 1964, **36**, 706–723.
61 S. Dhar, Z. Liu, J. Thomale, H. Dai and S. J. Lippard, *J. Am. Chem. Soc.*, 2008, **130**, 11467–11476.
62 B. Arunachalam, U. T. Phan, H. J. Geuze and P. Cresswell, *Proc. Natl. Acad. Sci. U. S. A.*, 2000, **97**, 745–750.
63 L. Ellis, H. Er and T. Hambley, *Aust. J. Chem.*, 1995, **48**, 793–806.
64 R. J. Amir, S. Zhong, D. J. Pochan and C. J. Hawker, *J. Am. Chem. Soc.*, 2009, **131**, 13949–13951.
65 H. Kühnle and H. G. Börner, *Angew. Chem., Int. Ed.*, 2009, **48**, 6431–6434.
66 H.-J. Li, J.-Z. Du, J. Liu, X.-J. Du, S. Shen, Y.-H. Zhu, X. Wang, X. Ye, S. Nie and J. Wang, *ACS Nano*, 2016, **10**, 6753–6761.
67 K. R. Barnes, A. Kutikov and S. J. Lippard, *Chem. Biol.*, 2004, **11**, 557–564.
68 R. Filosa, A. Peduto, S. D. Micco, P. d. Caprariis, M. Festa, A. Petrella, G. Capranico and G. Bifulco, *Bioorg. Med. Chem.*, 2009, **17**, 13–24.
69 H. Liu, Y. Li, Z. Lyu, Y. Wan, X. Li, H. Chen, H. Chen and X. Li, *J. Mater. Chem. B*, 2014, **2**, 8303–8309.

 